Water Research 267 (2024) 122543

Contents lists available at ScienceDirect

Water Research

journal homepage: www.elsevier.com/locate/watres

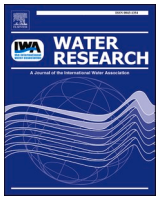

Functionalized composite nanofiber membranes for selective steroid hormone micropollutants uptake from water: Role of cyclodextrin type

Alessandra Imbrogno [a], Han Ya Lin [a], Akhil Gopalakrishnan [a], Babak Minofar [b], Andrea I. Schäfer [a,*]

[a] Institute for Advanced Membrane Technology (IAMT), Karlsruhe Institute of Technology (KIT), Hermann-von-Helmholtz-Platz 1, Eggenstein-Leopoldshafen 76344, Germany

[b] Department of Physical Chemistry, Faculty of Chemistry, University of Lodz, Pomorska 163/165, Lodz 90-236, Poland

ARTICLE INFO

Keywords:
Ultrafiltration
Inclusion complex
Adsorptive membranes
Macrocyclic host
Physio-chemical water treatment

ABSTRACT

Cyclodextrins (CD) entrapped in nanofiber composite membranes are potential selective adsorbing materials to remove steroid hormone (SHs) micropollutants from water. This study aims to elucidate the role of CD macrocyclic host type on the SHs inclusion complexation and uptake in filtration. Three CD types (α, β, and γ) are cross-linked with epichlorohydrin to form polymers (αCDP, βCDP and γCDP) and entrapped into a nanofiber composite membrane by electrospinning. TGA analysis confirmed the CD entrapment into the nanofiber without loss of CD molecules during filtration.

The CD type plays a dominant role in controlling the removal of different SHs. A similar removal (range 33 to 50 %) was observed with αCDP, irrespective of the SH type. In contrast, removal and uptake dependent on SH type were observed for β and γCDP, with the highest removal of 74 % for progesterone, followed by estradiol (46 %) and estrone (27 %) and the lowest removal of 3 % for testosterone.

Molecular dynamic (MD) simulation revealed a stronger and more stable complex formed with βCDP, as demonstrated by: i) the closer spatial distribution of SH molecules from the βCDP cavity and, ii) the quantum chemistry calculations of the lower de-solvation energy (+6.0 kcal/mol), which facilitates the release of water molecules from interacting interface of CD molecule and hormone. Regarding γCDP, the highest de-solvation energy (+8.3 kcal/mol) poses an energetic barrier, which hinders the formation of the inclusion complex. In the case of αCDP, a higher interaction energy (-8.9 kcal/mol) compared to βCDP (-4.9 kcal/mol) was obtained, despite the broader spatial distribution observed from the MD simulation attributed to a dominant hydrogen bonding interaction with the OH primary groups on the external surface cavity.

The findings highlight the relevance of the CD type in designing selective adsorbing membranes for steroid hormone micropollutant uptake. Experimental results and MD simulation suggest that βCD is the most suitable CD type for steroid hormone uptake, due to a more stable and stronger inclusion complexation than α and γCD.

1. Introduction

Natural or synthetic steroid hormones and pharmaceuticals used as contraceptives or to accelerate animal growth in livestock are persistent micropollutants spread in the aquatic environment (Cheng et al., 2020, Kamilya et al., 2023). The persistence of estrogenic micropollutants in water resources is a worldwide concern, due to its detrimental endocrine disruption effects on aquatic life and human health at trace level concentrations below 1 ng/L (Adeel et al., 2017; Wu et al., 2021). Several studies have reported the alteration of male and female reproductive systems, cardiovascular disease, thyroid malfunction, obesity and breast and prostate cancer (Bhandari et al., 2015; Diamanti-Kandarakis et al., 2009; Trasande et al., 2015; Zeeman, 1996). Steroid hormones are naturally excreted by humans and animals and enter into the water cycle predominantly through wastewater effluents and leachate from livestock (Bilal et al., 2021).

Adsorbing materials (such as activated carbon, zeolites and metal-based nano adsorbents), membrane pressure-driven processes (nanofiltration and reverse osmosis), advanced oxidation (such as ozone, UV-light, Fenton, electrochemical and photolysis) and microbial

* Corresponding author.
E-mail address: Andrea.Iris.Schaefer@kit.edu (A.I. Schäfer).

https://doi.org/10.1016/j.watres.2024.122543
Received 26 June 2024; Received in revised form 25 September 2024; Accepted 26 September 2024
Available online 27 September 2024

degradation in activated sludge are commonly applied in water treatment for removal of micropollutants (Bhatt et al., 2022, Nure and Nkambule, 2023, Saravanan et al., 2022, Xu et al., 2023). Steroid hormone micropollutants (SHs) are mostly retained by size exclusion with nanofiltration/reverse osmosis (NF/RO), resulting in variable removal (range 40–95 %) caused by uncontrolled adsorption and further diffusion through the membrane (Imbrogno and Schäfer, 2021; Schäfer et al., 2011; Xu et al., 2023). More advanced processes capable of removing micropollutants from water through selective and controlled adsorption, without compromising the water permeability, are required (Nure and Nkambule, 2023). Combining conventional membrane filtration with adsorbing materials is a promising advanced membrane technology suitable for pollutant removal from water (Dalanta et al., 2023). Some examples of such advanced processes have been reported in the literature to achieve an effective removal of micropollutants from water, using as adsorbents activated carbon, carbon nanotubes and anion exchange particles (Nguyen et al., 2021; Tagliavini and Schäfer, 2018; Uebele et al., 2022; Zhang et al., 2020). Macrocyclic hosts, such as crown ether, cyclodextrin, calix[n]arene and pillar[n]ene, have been tested as adsorbent materials in water purification and resource recovery mostly in batch studies, due to highly selective and reversible binding with ions, dyes and organic micropollutants (Guo et al., 2021; Lin et al., 2024b; Ma et al., 2020; Sikder et al., 2019; Zhou et al., 2022). The reversible binding of organic solutes with macrocycles offers the advantage of regeneration after saturation. The most used methods for regeneration are based on organic solvents (e.g. ethanol or methanol) with an adsorption efficiency in a range from 75 % to 90 % (Ghosh et al., 2013; Jiang et al., 2017; Lee and Kwak, 2019; Lin et al., 2019; Ozelcaglayan and Parker, 2023; Wang et al., 2019;). Alternatively, a reversible binding of CD on a membrane using a UV-sensitive cross-linker, was explored to avoid the use of solvents (Dong et al., 2020.

The macrocyclic host is a supramolecular structure containing a cavity, which exhibits the molecular recognition ability of guest targets by ionic interactions, hydrogen bonds and hydrophobic interactions (Ma et al., 2020). Cyclodextrins (CD) are cyclic oligosaccharides with a conical shape and different cavity diameters (see Fig. 1A). Among various types of macrocyclic hosts, CDs have received dominant attention as a novel adsorbent material suitable for water purification from pollutants, due to their ability to form inclusion complexes with the majority of emerging micropollutants, including steroid hormones (Alsbaiee et al., 2016; Kamaraj et al., 2024; Morin-Crini et al., 2018; Ozelcaglayan and Parker, 2023; Tian et al., 2021). Three types of CDs are most common, namely αCD, βCD and γCD, which are composed of six, seven and eight glucopyranoside units, respectively (Del Valle, 2004). Despite the existence of larger CDs containing from 9 up to 12 units, namely δ-CD, which has been proven by crystallographic evidence after extraction from the bacterial strain, these larger macrocycles are not commercially available (Del Valle, 2004; Szejtli, 1998). These three CD types show a different diameter of the hydrophobic cavity of 0.6 nm (αCD), 0.8 nm (βCD) and 0.9 nm (γCD), determined by X-ray diffraction (Ding et al., 1991; Szejtli, 1998). The cavity diameter is flexible and a structural variation of CDs hosts and cavity dimension have been observed in molecular dynamic simulation and H—NMR spectroscopy in presence of water molecules (Ganjali Koli and Fogolari, 2023; Raffaini and Ganazzoli, 2007; Sandilya et al., 2020; Vicatos et al., 2022). The cavity diameter variation is caused by the CD hydration, which means the penetration of water molecules into the cavity and the formation of hydrogen bonding with the OH groups. According to a study by Raffaini and Ganazzoli (2007), the number of water molecules that can be accommodated in the cavity is 4, 6 and 9 for α, β and γCD, respectively, determined from the pair distribution function around the centre of the macrocyclic host. This results in a hydrated cavity diameter of 0.9, 1.0 and 1.2 nm for α, β and γCD, respectively, determined as a trajectory between a single pair of glycosidic oxygens in the cavity during the MD simulation in water. Considering that the Stokes sphere diameter of natural SHs is of the order of 0.8 nm (Bridle et al., 2016), it is expected that a different number of SH molecules can be accommodated within the cavity of the three CD types. When neutral organic molecules, such as SHs, are present in the solution, the water molecules in the cavity are replaced by the hydrophobic guest molecule (Ganjali Koli and Fogolari,

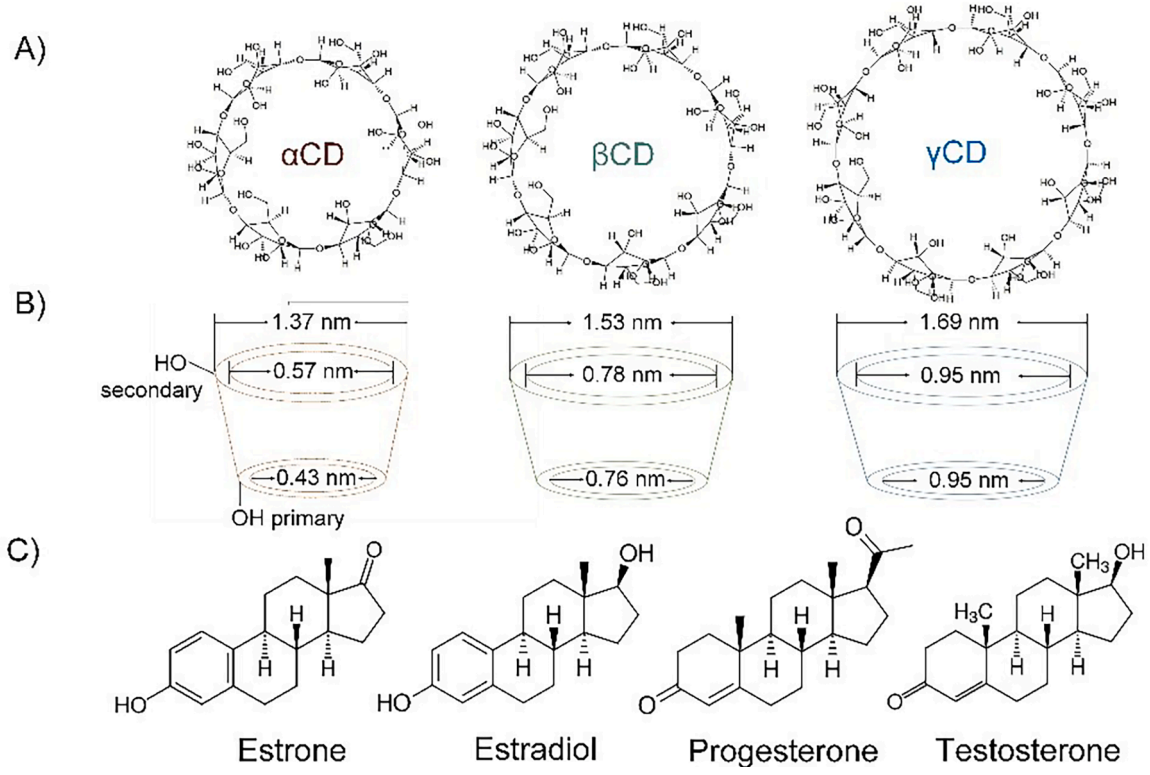

Fig. 1. Schematics of chemical structures of A) α, β and γCDs, and C) steroid hormones, B) inner and outer diameter of the CD cavities.

2023; Rekharsky and Inoue, 1998; Sandilya et al., 2020).

Binding of the guest molecule within the macrocyclic host involves three energetic steps: i) de-solvation of the guest molecules, ii) removing the water molecules in the cavity of the macrocyclic host, and iii) interaction of the guest molecule to replace the water molecules within the cavity by hydrogen bonding, van der Waals or Coulomb interactions (that is electrostatic interactions) (Abarca et al., 2016). To remove water molecules from the CD cavity a certain energy is required which is called de-solvation energy. Solvation or de-solvation energy is defined as the energy difference between the solvated (water-CD complex) and un-solvated CD molecule (Gholami et al., 2024). The interaction energy is the total energy contributing to the binding of the guest molecule to the macrocyclic host (including the contribution of the hydrogen bonding, van der Waals and Columbic interactions) (Gholami et al., 2024). The host-guest complexation is driven by a chemical potential gradient, where the chemical potential of the guest molecule solvated in water is the same as the guest molecule bound to the macrocyclic host solvated in water (Buchwald, 2002). This means that for organic guest molecules with weak hydration shells, the inclusion complexation is favoured, as the energy required to de-solvate the guest molecule is compensated by the energy gained from the complexation into the macrocyclic host (de Oliveira and Ben-Amotz 2019; Spencer et al., 1998). Organic molecules properties (such as dipole, hydrophobic and hydrophilic functional groups) can affect hydration. A weaker hydration can be expected for SHs due to a level of hydrophobicity (log k_{ow} between 3 and 4) and uncharged structure at natural water pH (10.2 < pKa <10.7) (Lewis and Archer, 1979; Waring, 1983). Indeed, the dominant interactions of the inclusion complexes between SHs with the CD cavity are hydrophobic and hydrogen bonding (Ganjali Koli and Fogolari, 2023; Lin et al., 2022). A molecular electrostatic potential topography study revealed that the hydrogen bonding interactions with the oxygen of the secondary OH groups (see Fig. 1B) within the ring of βCD and γCD results in a "barrel-like" structure, where the guest molecule penetrates into the cavity, while for αCD, the hydrogen bonding interactions occur mostly with the primary OH groups external to the macrocyclic host structure (Pinjari et al., 2006). Another study by Gholami et al. (2024) investigated the H-bonding interaction mechanisms of hydrocortisone with CDs by molecular dynamic simulations and found that hydrogen bonding occurs mostly between the hydroxyl groups of CDs and the ketone groups, with a full intramolecular bonding in the βCD cavity, leading to a more rigid structure and lower solubility than αCD and γCD.

Previous studies investigated the uptake of SHs by different CD types and revealed controversial results. For instance, one study (Tang et al., 2018) investigated the adsorption of 17β-estradiol (E2) and 17α-ethinylestradiol (EE2) by βCD and γCD. The highest adsorption capacity was observed for γCD, which has been explained by the larger complexation ratio of 1:2 between γCD and E2 molecules, while the βCD complexation ratio was 1:1. A different finding has been published by Shakalisava and Regan (2006), who reported that the adsorption of SHs by γ and βCD is controlled by the functional group types, which affect the association constants (related to the strength of interaction between the macrocyclic host and the guest molecule), while the complexation ratio is the same at 1:1. Indeed, the association constants (hence the inclusion complexation) in the cavity of γCD are larger for organic molecules with aromatic hydroxyl groups (estriol, EE2, E2 and estrone), which can penetrate deeply into the larger cavity of γCD, compared to βCD (Shakalisava and Regan, 2006). In contrast, other studies (Moulahcene et al., 2015; Oishi and Moriuchi, 2010; Oishi et al., 2008) reported a similar uptake of E2 and progesterone with βCD and γCDP because of the formation of an inclusion complex. The interaction with αCD has been attributed to adsorption to the polymer matrix, without inclusion-complex formation in the CD cavity, as shown in the lower variation of the E2 absorption spectrum determined by UV–vis.

The uptake of other micropollutants, such as pesticides (e.g. atrazine and chlordecone), poly-cyclic aromatic hydrocarbon (e.g. phenanthrene), pharmaceuticals (e.g. pimavanserin) and phenolphthalein has been investigated with α, β and γCD (Hemine et al., 2020; Kayaci et al., 2013; Lu et al., 2020; Rana et al., 2016; Romita et al., 2019). An overview of studies on the uptake of various micropollutants by the three CD types is reported in Table S1. The results show various adsorption capacities of the three CDs, which has been, in most cases, explained by a different penetration into the CD cavity, without a consistent trend for the three CDs. Overall, deeper penetration into the CD cavity and higher uptake have been reported with γ and βCD, when pollutants with larger molecular weight (> 300 Da), such as chlordecone, phenolphthalein and pimavanserin (molecular weight above 300 Da) are tested (Hemine et al., 2020; Lu et al., 2020; Rana et al., 2016). In contrast, smaller pollutants with a molecular weight below 200 Da (such as atrazine and phenanthrene) can form an inclusion complexes independently of the CD type (Kayaci et al., 2013; Romita et al., 2019). These studies highlight that the inclusion complexation is strictly dependent on the CD cavity and pollutant characteristics, limiting the investigation at batch conditions. Further investigation is required to elucidate the role of CD type on the inclusion complexation of micropollutants during filtration, where the hydraulic residence time limits contact with the pollutant compared to batch adsorption.

To investigate the role of different CD types on the inclusion complex formation and uptake of micropollutants, such as SHs, under water filtration conditions, it is necessary to entrap the cross-linked CD molecules within a nanofiber mat in a composite membrane. The nanofiber mat provides larger surface area and high porosity (Liu et al., 2020). In a previous study (Imbrogno et al., 2024a), epichlorohydrin cross-linked βCD was successfully entrapped in a polyethersulfone nanofiber matrix deposited on an ultrafiltration (UF) membrane. A UF membrane is selected to provide i) mechanical support for the nanofiber matrix when applied to water filtration, ii) pathogen retention which is essential in water treatment (Baker, 2004) and iii) higher water flux than other pressure-driven membrane processes applied for MP removal, such as NF/RO (Mulder, 2012). In a previous study (Imbrogno et al., 2024a), the inclusion complexation of natural SHs with cross-linked βCD was investigated experimentally during filtration, to identify the limiting factors controlling SH uptake. Molecular dynamic simulation revealed a different affinity of SHs for the βCD macrocyclic hosts, with progesterone showing the strongest inclusion complex formation. This study aims to move a step forward in exploring the role of the CD type in controlling SH uptake during filtration, as well as the inclusion complex formation and affinity of different SHs towards the macrocycles. To address this objective, the following three research questions are answered: i) How does the steroid hormone chemical structure affect the uptake by α, β and γCD type and the interaction with the cavity? ii) What is the role of CD type (α, β and γCD) on the inclusion complex formation with steroid hormones? iii) What is the energetic limiting step (de-solvation and interaction energy) for the inclusion complex formation with different CD types? Various experimental parameters, such as SH concentration and type (estradiol, estrone, testosterone and progesterone), feed flow rate (hence flux and hydraulic residence time) and nanofiber matrix thickness are investigated to evaluate SH uptake and removal when α, β and γCD are individually entrapped in polyethersulfone nanofiber matrix by cross-linking with epichlorohydrin in a nanofiber composite membrane (CNM). The experimental results are compared with molecular dynamic simulation and quantum calculation to gain insights into the inclusion of complex formation of the four SH types with the three CD types and the energetic barriers.

2. Materials and methods

2.1. CD cross-linking conditions

The cross-linker, epichlorohydrin (EP, purity ≤ 100 %, Sigma-Aldrich, Germany) and three types of cyclodextrins, namely, α-cyclodextrin (αCD, 98 %, Merck, Germany), *β*-cyclodextrin (βCD, 98 %,

Thermo Fisher Scientific, Germany) and γ-cyclodextrin (γCD, 90 %, Sigma-Aldrich, Germany) were used for CD cross-linking reaction. Sodium hydroxide (NaOH, 97 %, Merck, Germany) was used as an alkaline catalyst for deprotonation during the cross-linking reaction. The polymerization of CD with EP was adapted from previous studies (Heydari et al., 2018; Renard et al., 1997). A solution containing 1 g of CD (αCD, βCD or γCD individually dissolved) and 1.6 mL of NaOH (33 %) was stirred for 24 h at 23 °C, controlled by a temperature controller (Sunlab, SU 1300, Germany). Subsequently, 0.68 mL of EP was individually added to the solution of CD and NaOH and heated to 30 °C for 3 h and 50 min. Acetone was added to the solution and removed subsequently by decantation. The pH of the CD solution obtained was adjusted to 12 with HCl (6 N). The CD solution was then heated up to 50 °C for 24 h for cross-linking. After cooling, the solution was neutralized with 6 M HCl and dialyzed for 2 days using a dialysis membrane (Spectra/Por® 6 MWCO 1000, 45 mm, Spectrum Lab, Thermo Fisher Scientific, Germany). The CD solution was dried in the oven at 80 °C for 12 h. The dried CD polymer was then crushed using a ceramic mortar and used to prepare the electrospinning solution.

2.2. Membranes and nanofiber electrospinning

Polyethersulfone UF membrane (Biomax 100 kDa, PBHK, Millipore, Bedford, USA) was used as the support for the electrospun nanofiber matrix. Polyethersulfone powder (PES, Veradel 3000P, Solvay, Belgium) and *N, N*-dimethylformamide (DMF, 99 %, Sigma-Aldrich, Germany) were used to prepare the electrospinning solution for the nanofiber preparation following the conditions reported in previous studies (Askari et al., 2023; Homaeigohar et al., 2010). The electrospinning solution was prepared by dissolving 25 wt/v% of PES in DMF at 40 °C for 18 h, with the 30 % loading of cross-linked CDP (individual αCDP, βCDP or γCDP, corresponding to 15 g/m^2). A total of 3 mL of the solution was electrospun on the active layer of the UF membrane with a 5 mL syringe by a vertical setup of the electrospinning equipment. A syringe pump (Model LA100, Landgraf Labor system HLL GmbH, Germany) was used to control the flow rate at 0.8 mL/h. The needle tip-to-collector distance was set at 15 cm for αCDP and βCDP from the collector in the horizontal stage with an x-y controller (SMC 200, MOVTEC Wacht GmbH, Germany). Since a reduction of membrane permeability was observed when the same distance was used to prepare the nanofiber containing γCDP, the tip-to-collector distance was increased to 20 cm. The electrospinning voltage was fixed at 17 kV (Model HPC-14–20,000, FuG Elektronik GmbH, Germany).

2.3. Characterization of the composite nanofiber membrane

An analysis of nanofiber morphology was performed with a scanning electron microscope (SEM, Zeiss-REM Supra 60VP equipped with SE-ll detector) to evaluate the nanofiber diameter and the matrix cross-section with a voltage of 5 kV. A 10 nm gold layer was coated on a dried membrane coupon using a sputter coating machine (Bal-Tec 005 Coating System, Bal-Tec, Germany). The cross-section sample coupon was prepared by breaking the membrane coupon in liquid nitrogen (nanofiber matrix and UF support, separately). The average diameter of the nanofibers was estimated from the SEM images using ImageJ (v 1.54d) software and the scale bar of the SEM images was set as a reference for the measurements (see Fig. S4). Fourier transform infrared spectrometer (FTIR, spectrometer from 4000 to 400 cm^{-1}, 64 scans, and resolution 4 cm^{-1}, Spectrum Two, PerkinElmer, Germany) was used to confirm the cross-linking reaction between CDs and epoxy.

A thermogravimetric analyser (TGA, TG 209 F1 Libra, Netsch, Germany) was used to verify the immobilization of CDP in the nanofiber matrix after electrospinning and water flux filtration (Nielsen et al., 2011). The nanofiber samples were heated from 30 to 900 °C at a constant heating rate of 10 °C/min under a nitrogen atmosphere and the weight loss variation was recorded. Calibration was performed using nanofiber samples containing 30 % CDP loading and different initial masses, to confirm that the CDP was successfully entrapped in the nanofiber matrix without leaching after water filtration. The initial masses were weighted with a semi-micro balance (Explorer EX225D/AD, Ohaus, Germany) in a range between 0.5 and 10 mg. A calibration curve was obtained by plotting the mass weight loss (%) at different initial masses and the weight loss was quantified. All nanofiber samples were heated to 110 °C under a nitrogen atmosphere for 10 min to remove residual water in the nanofiber before TGA measurement.

2.4. Steroid hormone micropollutants and solution chemistry

Radiolabeled [2,4,6,7-^{3}H] Estrone (E1, 3.48 TBq/mM), [2, 4, 6, 7–^{3}H] β-estradiol (E2, 2.59 TBq/mM), [1,2,6,7-^{3}H] progesterone (P, 3.63 TBq/mM), and [1,2,6,7-^{3}H] testosterone (T, 2.94 TBq/mM) were used as steroid hormone (SH) micropollutants and purchased from Perkin Elmer, USA. The radiolabeled hormones were used at a concentration varying from 10 to 100 ng/L. For E2 concentrations above 100 ng/L, non-radiolabeled estradiol (≥98 % purity, purchased from VWR Chemicals, Germany) stock solution of 10 μg/L was mixed with a solution containing 100 ng/L of radio-labeled E2. An electrolyte background solution containing 1 mM $NaHCO_3$ (Bernd Kraft, Germany, 99.7 % purity) and 10 mM NaCl (VWR Chemicals, Germany) was used to prepare the feed solutions containing SH.

2.5. Steroid hormone analysis

A liquid scintillation counter (LSC, 4910 TR, Perkin Elmer, USA) was used to measure the tritium radioactivity of the aqueous solutions containing radio-labeled steroid hormones. The concentration was determined by using a calibration curve obtained with standard hormone solutions of known concentration (Bridle et al., 2016). The calibration curve in the range of concentrations between 0.1 and 100 ng/L and the limit of detection at 0.1 ng/L are shown in Fig. S2. LSC analysis was performed by mixing 1 mL of aqueous hormone solution with 1 mL of a scintillation cocktail (Ultima Gold LLT, Perkin Elmer, USA).

2.6. Molecular dynamic simulation

Molecular dynamic (MD) simulations were performed to evaluate the spatial distribution of SH molecules around the CD (αCDP, βCDP or γCDP) cavity and the inclusion complexation formation. The GROMACS 2020 simulation package and the General AMBER Force Field (GAFF) were used for the simulations (Hess et al., 2008; Van Der Spoel et al., 2005). A random distribution of βCDs and SH molecules was constructed in the simulation boxes using the Packmol program (Martínez and Martínez, 2003; Martínez et al., 2009). The simulations were performed using a single cross-linked molecule of CD (αCDP, βCDP or γCDP) and ten molecules of SH (ratio 1:10) solvated in water. The epoxy group of EP was terminated with methyl and hydroxyl groups. To perform the MD simulation, SH molecules at a concentration of 6.7 mM (corresponding to about 2 g/L) were used. This concentration is not representative of the experimental conditions performed at about two orders of magnitude lower (from 0.01 to 1000 μg/L) than the simulation conditions. However, simulation of SH—CD complexation with a significant number of water molecules and SH at trace level concentrations is not practical, as it requires huge computation resources. Other simulation conditions, such as simulation time, temperature and pressure control for system equilibrium are similar to previous work (Imbrogno et al., 2024a). The radial distribution function, RDF or g(r), was determined to evaluate the spatial distribution of four types of SH molecules (progesterone, testosterone, estrone and estradiol) from the center of α, β and γCD cavity. When different CDs were used, the RDF obtained individually for each of the ten SH molecules was summed up to have one RDF representative of SH molecule distribution in the proximity of the CD (αCDP, βCDP or γCDP) cavity.

Quantum calculations (QC) were used to extrapolate the de-solvation energy of the cross-linked αCDP, βCDP or γCDP in water and the interaction energy for the inclusion complex formation with estradiol to elucidate the energetic limiting step for the different CD types. The interaction and de-solvation energies were determined by QM calculations using the density functional theory (DFT) with M06–2X functional (Zhao and Truhlar, 2008) implemented in the Gaussian 09 program (Frisch, 2009). The interaction energy is negative when energy is required to separate the interacting guest molecule and macrocyclic host, while a positive value is an indication that energy is released when the complex is separated. A stronger interaction of the guest-complex, results in a more negative value of the interaction energy. The geometries generated by MD simulations were taken and re-optimized by M06–2X with a 6–31 G basis set. The gas phase interaction energies were calculated for the geometries taken from the MD simulation by M06–2X DFT functional with a cc-pVTZ basis set. The basis set superposition error (BSSE) of gas-phase interaction energies was corrected by the counterpoise method (Boys and Bernardi, 1970). Additionally, the effect of solvation was calculated using the implicit solvation model SMD (Marenich et al., 2009).

2.7. Static adsorption protocol

Static adsorption was performed to evaluate the SH adsorption capacity of the nanofiber matrix and determine the adsorption isotherm. Static adsorption experiments were performed with E2 for two main reasons: i) it is the most representative SH micropollutant reported in the watch list of the 2022 European Commission (European Parliament, 2022), and ii) it has a steroidal structure similar to the other three SHs (estrone, testosterone and progesterone). The experiments were performed with different E2 concentrations (0.01, 0.1, 1, 10, 100, and 1000 μg/L) and CNM coupons of 25 mm diameter. The coupons were soaked in 100 mL of E2 solution using an incubator shaker (Innova 43 R, New Brunswick Scientific, USA) at 260 rpm and a temperature of 20 °C. The variation of E2 concentration in the solution was evaluated at different times (0, 0.1, 0.2, 0.5, 1, 2, 3, 4, 5, 6, 7 and 24 h; unfortunately, 26 h was omitted) using a sample of 2.5 mL volume for the LSC analysis. The equations for calculating steroid hormone removal (R, %) and uptake (q_{ads}, ng/cm^2) are reported in Table S4.

2.7. Steroid hormone filtration protocol

Filtration experiments were performed in a dead-end stirred cell system composed of 3 Perspex cells in parallel (volume 10 mL, Millipore, Modell 8010, Germany). Details of the system are shown in Fig. S1. A peristaltic pump (MFLX 07,528–10, Masterflex, Germany) was used to control the feed flow rate. The permeate mass during filtration was measured with balances (AX822/E, Ohaus, USA), while the pressure and temperature applied in the feed were monitored by pressure (PT5415, IFM, Germany) and temperature (TA2145, IFM, Germany) sensors, respectively. Filtration experiments were performed with membrane coupons of 2.5 cm dimeter and an effective surface area of 3.8 cm^2. Filtration protocol is described in Table S3. To quantify SH uptake during filtration, the breakthrough curve of four SHs was determined with the three CD types under varying operating conditions. Specifically, the uptake and removal were investigated at different feed flow rates (hence flux and hydraulic residence time), nanofiber matrix thickness and hormone concentration. The equations for calculating steroid hormone removal (R, %), uptake (q_{ads}, ng/cm^2), water flux (J_0, L/m^2.h) and hydraulic residence time (t_r, s) are reported in TableS3. The experimental error of such parameters was determined by identifying the major contributing error sources and applying the error propagation method (Imbrogno et al., 2024b). Details of the error analysis and calculated errors are reported in Tables S5–S8.

3. Results & discussion

SH uptake and removal were assessed in static conditions and further investigated during filtration to elucidate the role of CD type (α, β and γ) and hormone type (E2, E1, P, T) on the uptake and removal under varying conditions of fluxes (hence hydraulic residence time), nanofiber matrix thickness (hence fibre surface area) and hormone concentration. MD simulation and QC calculation provided new insights on the inclusion complex formation between SH and the three CD types and the energetic barrier.

3.1. CD type cross-linking and nanofiber matrix morphology

α and γCD type cross-linking with EP was analysed by FT-IR and TGA to verify the occurrence of the cross-linking reaction and the entrapment in the nanofiber matrix before and after filtration. For βCD, the FT-IR spectra and TGA analysis were published in the previous study (Imbrogno et al., 2024a).

The occurrence of cross-linking reactions between the hydroxyl groups of α and γ CD and the epoxy rings of EP was confirmed by FT-IR (Fig. 2A, B). In Fig. 2A, the O—H stretching peaks observed at 3550–3200 cm^{-1} confirmed the occurrence of secondary alcohol produced by the epoxide ring-opening reaction, similar to the spectra observed for βCD. Similar FT-IR spectra were expected due to the similar chemical structure of the three CD types with OH functional groups involved in the cross-linking reaction. Another peak for C—H stretching and bending at 2915 and 1456 cm^{-1} confirmed the formation of methylene groups (Celebioglu et al., 2019; Gidwani and Vyas, 2014). In Fig. 2B, the peaks observed at 1079 and 1023 cm^{-1} for α and γCD were attributed to C—O stretching, which was used to analyse the transformation from primary to secondary alcohol after cross-linking, the peak's absorbance ratio (Celebioglu et al., 2019). The absorbance ratios (A_{1079}/A_{1023}) for αCD and γCD were both found to be 0.46. After cross-linking, the absorbance ratios (A_{1079}/A_{1023}) for αCDP and γCDP increased to 0.50 and 0.59, confirming the formation of secondary alcohols.

The nanofiber morphology (Fig. 3A–C) and membrane cross-section (Fig. 3D–F) of the CNM membranes containing α, β and γCD (Fig. 3A–F) were visualized by SEM to measure the nanofiber diameter and the nanofiber matrix thickness.

Fig. 3A–C shows the smooth morphology of nanofiber for αCD, βCD and γCD and average diameters of 283 ± 109, 310 ± 95, and 289 ± 116 nm, were measured, respectively (nanofiber diameter distribution is shown in Fig. S4). The nanofiber matrix thickness (Fig. 3D–F) was similar for the CNM containing different CD types with an average values of 182 ± 8, 272 ± 17 and 152 ± 38 μm for αCD, βCD and γCD, respectively. Increasing the electrospinning cycles, the nanofiber matrix thickness increased to 412 ± 21, 305 ± 17, and 530 ± 90 μm (see Fig. S5). The water permeability of the CNM membranes containing αCD, βCD and γCDs was not affected by the nanofiber matrix deposition as shown in Fig. S6, with an average value of 508 ± 60 L/m^{2}h.bar. This is a plausible result due to the insignificant additional resistance of the highly porous nanofiber matrix thickness deposited on the UF membrane.

TGA analysis of CNM membranes containing α and γCDP was performed to verify the presence of the cross-linked CDs in the nanofiber matrix after electrospinning and water filtration. The results for α and γCD are reported in Fig. 4. TGA analysis for βCD was published in the previous study (Imbrogno et al., 2024a). An insignificant variation of weight loss of 63 ± 2 and 62 ± 2 % was observed for α and γCD before and after pure water flux, respectively, confirming the presence of cross-linked α and γCDs in the nanofiber matrix thickness. The trend of weight loss with the initial decrease of mass in the temperature range between 400 and 600 °C is consistent with another study, where it is referred to the decomposition of PES nanofiber (Askari et al., 2023).

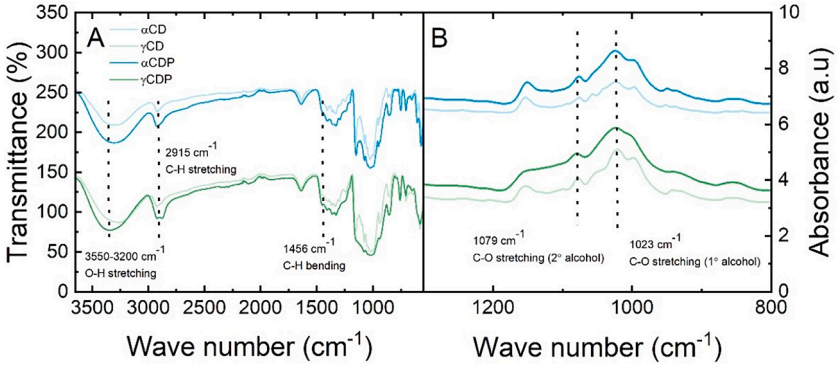

Fig. 2. FTIR of (A) before and after cross-linked α, β and γ CD and (B) zoom-in of C—O stretching. βCD spectrum is adapted from Imbrogno et al. (2024a).

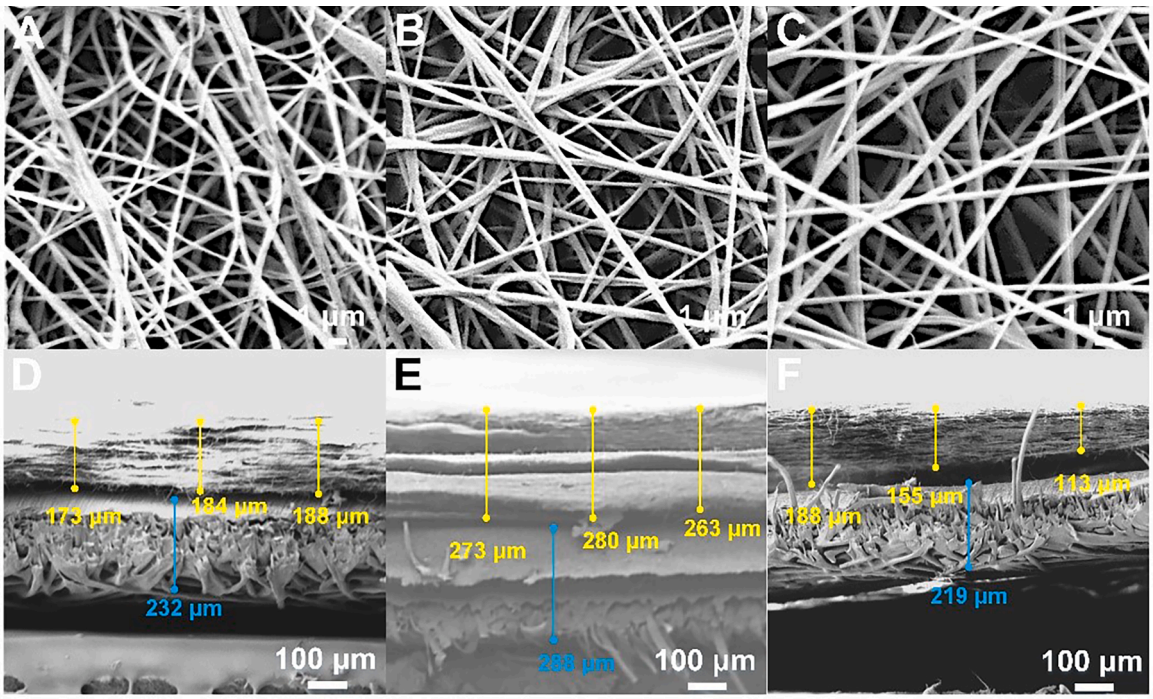

Fig. 3. A–C) Surface and D–F) cross-section of αCD, βCD and γCD CNMs, respectively. (15 g/cm^2 CDP, 4 electro-spinning cycles, blue line: pristine UF membrane thickness; yellow line: nanofiber matrix thickness). (For interpretation of the references to colour in this figure legend, the reader is referred to the web version of this article.)

3.2. Static steroid hormone adsorption uptake and isotherms by different CD types

In the first instance, estradiol uptake by different CDs (α, β, and γCDs) was investigated to assess the role of CD type on E2 uptake and saturation in static conditions. E2 uptake and removal by the different CD types are shown in Fig. 5A, B. E2 removal increased over time until equilibrium was reached after about 6 h, with values in the range of 70 to 80 % for the three CD types, which is about 2.6 times higher than the UF pristine membrane. At equilibrium E2 uptake reached similar values of 2.5 ng/cm^2 for the βCD and 2 ng/cm^2 for α and γCD. These results show an insignificant difference in E2 removal and uptake for the different CD types when tested in static conditions. This finding is in contrast to a previous study (Tang et al., 2018), who reported a higher adsorption capacity of E2 with γCD than βCD when tested in batch condition. This was attributed to a deeper penetration of E2 molecules within the γCD forming an inclusion complexation ratio of 1:2, while for βCD, the ratio was 1:1. Two reasons can explain the different result, i) the batch experiment was performed at a high E2 concentration in the range of 0.4 g/L, which is about 7 order of magnitude higher than the concentration (1•10^{-7} g/L) applied in this work, and ii) cross-linked CDs were mixed directly with E2 solution, while here the cross-linked CD molecules were entrapped into a nanofiber matrix, which provided a mass transfer limitation to the adsorption of E2 molecules by the CDs. This hypothesis is supported by another study (Kayaci et al., 2013), where a similar uptake of phenanthrene by the three CD types immobilized into a polyethylene nanofiber matrix was observed in batch conditions.

E2 adsorption isotherm with different CD types was investigated to evaluate whether adsorption saturation was reached at equilibrium. The results are shown in Fig. 5C, D. E2 uptake increased linearly with equilibrium concentration from 0.01 to 1000 µg/L (Fig. 5D) irrespective of the CD types, indicating that saturation of CD molecules was not reached in the experimental concentration range. The adsorption isotherm followed the Freundlich model for the three CD types, with similar estimated *k* values (hence adsorbing loading) in the order of 1.9 to 2.9 µg/g (calculated parameters are shown in Table S10). This result highlights that similar and equally high uptake is achievable for E2 by

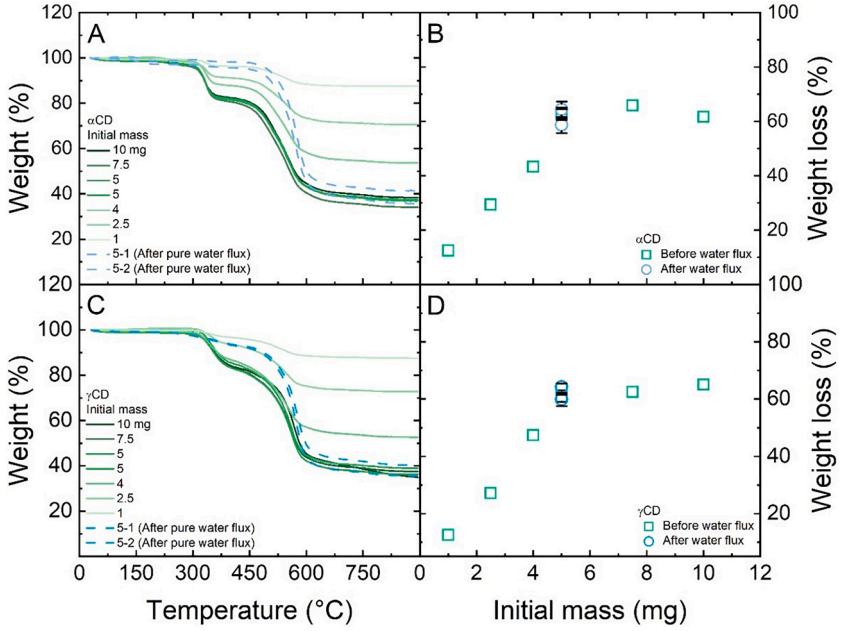

Fig. 4. TGA analysis (N_2 atmosphere, 30 to 900 °C, heating rate of 10 °C/min) nanofiber matrix, (A, B) αCD and (C, D) γCD.

the three CD types in batch conditions, where uptake is mostly limited by the E2 diffusion mass transfer in the bulk solution. In the next step, the role of CD type on SH uptake was investigated under filtration conditions (hence limited contact time) and with different SHs.

3.3. Role of CD type on steroid hormone uptake and removal during filtration

The variation of E2 permeate to feed concentration ratio over time (breakthrough curve, Fig. 6A–C) was used to determine the contribution of CD type on uptake and removal during filtration.

No equilibrium was reached in the breakthrough of the CNM membrane. A permeate-to-feed concentration ratio (Fig. 6A) was reported irrespective of the CD type, suggesting that the membrane was not saturated. This is consistent with the similar E2 uptake of 7.3 ng/cm^2 for γCD and 9.0 ng/cm^2 for α and βCD (Fig. 6B) as well as similar E2 removal of 32 % for γCD, 42 and 46 % for α and βCD (Fig. 6C). These results indicate that E2 adsorption and removal were similar for the three CD types, which is consistent with the similar trend of removal and uptake observed for E2 in static conditions. Previous studies reported similar findings for the uptake of E2 (Moulahcene et al., 2015; Oishi and Moriuchi, 2010; Oishi et al., 2008) and other pollutants with similar molecular weight (atrazine and phenanthrene) (Kayaci et al., 2013; Romita et al., 2019)by βCD and γCD, which was attributed to the formation of inclusion complex irrespective of the CD type. To elucidate whether the hormone type plays a role in controlling the uptake by the three CD types, the removal of four SHs and uptake was investigated in the next step.

3.4. Role of steroid hormone type on the uptake by different CD type

The removal and uptake of various SHs, namely estradiol (E2), estrone (E1), progesterone (P) and testosterone (T), by the CNM membranes containing cross-linked α, β and γCDP were investigated to determine whether SHs chemical characteristics affect the CD interaction and consequently, adsorption. The results are shown in Fig. 7A and B.

The results revealed a different trend of removal and uptake for the four SHs and the three CD types, suggesting that the SH chemical structure affects the interaction with α, β and γCD. Similar removal and uptake were observed for P, T and estrogens E1 and E2 (33, 34, 42 and 50 %, respectively) when CNM membrane containing αCDP was used, consistently with a similar uptake in the range of 7.4 to 8.7 ng/cm^2. This indicates that, SH interaction with αCDP is independent of SH chemical structure. In contrast, removal and uptake dependent on hormone type were observed when CNM membrane coupons containing β and γCDP were used. Specifically, when P was filtered through the membrane, the highest removal of 74 % and uptake of 11.1 ng/cm^2 were obtained with βCD, followed by E2 (46 %) and E1 (27 %), while the lowest removal and uptake of 3 % and 2.3 ng/cm^2, respectively, were observed for T when CNM membrane with γCDP was used. A previous study (Oishi and Moriuchi, 2010) reported a stronger uptake of E2 by βCD and γCD, due to the inclusion complex formation, while for αCD, the complexation did not occur as no change in the fluorescence absorbance spectra was observed. The highest reduction of the fluorescence intensity was observed with βCD, which was attributed to the formation of a more stable inclusion complexation than γ and α. These findings from the literature support the similar removal and uptake observed with αCDP, which was independent of SH type. Other studies investigated the association constants of SHs with β and γCD, which revealed that the chemical structure of SHs affected the association constants, and hence the strength of the inclusion complex formation (Lin et al., 2022; Sadlej-Sosnowska, 1997; Shakalisava and Regan, 2006). According to these studies, the phenyl rings of estrogens are the functional groups able to penetrate deeply into the CD cavity, and they are involved in the inclusion complexation with β and γCD. Regarding T and P, the interaction with β and γCD is mostly attributed to hydrogen bonding and the penetration into the cavity is weaker due to the absence of phenyl rings. This finding supports the low T removal and uptake observed with β and γCD. The experimental results and the findings reported in the literature highlight the significance of the SH's chemical structure in controlling the interaction with the different CD types and possibly the formation of the inclusion complex.

3.5. Inclusion complex dynamics and energy for different CD types

To gain insights into the role of CD types in the inclusion complex formation with different SHs and the energetic limiting step, MD simulations and QC calculations were performed. The spatial distribution of SH molecules around the cavity of α, β and γCDP was investigated to

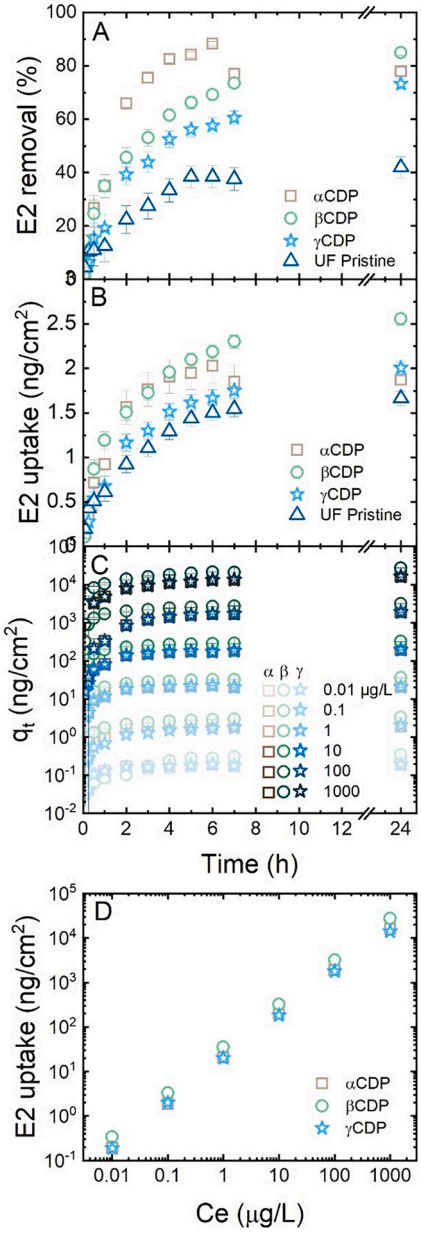

Fig. 5. A) E2 removal, B) uptake and C, D) adsorption isotherm in static conditions by the composite nanofiber membrane determined with different CDs and E2 concentrations (260 rpm, pH 8.1 ± 0.2, 20 °C, 1 mM $NaHCO_3$, 10 mM NaCl, 15 g/cm^2 CDP). Data for βCD are adapted from Imbrogno et al. (2024a).

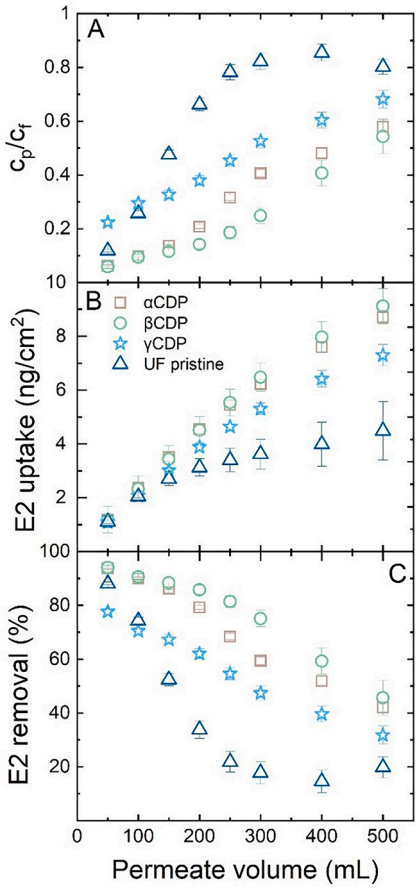

Fig. 6. A) E2 breakthrough curve showing the ratio of permeate to feed concentration, B) hormone uptake, and C) E2 removal as a function of permeate volume for the CNM with different types of CDs (3.8 mL/min, 22.5 ± 1.7 °C, pH 8.1 ± 0.2, 1 mM $NaHCO_3$, 10 mM NaCl, E2 100 ng/L). Data for βCD are adapted from Imbrogno et al. (2024a).

determine the inclusion complex ratio. The radial distribution function of SHs is shown in Fig. 8.

A higher peak of the radial distribution function was observed for E2 and P in the presence of βCDP with a radial distribution of about 0.5 nm, which is within the βCD cavity diameter of 1.0 nm in water (Raffaini and Ganazzoli, 2007). This is an indication that among ten SH molecules, at least one entered the cavity confirming a complex ratio of 1:1 for βCD (radial distribution of ten E2 molecules as an example is shown in Fig. S12). The complex ratio is consistent with the literature (Lin et al., 2022; Shakalisava and Regan, 2006; Tang et al., 2018) and with the higher removal observed experimentally for βCD in Fig. 7. A weaker peak intensity and a broader spatial distribution of SH molecules, were observed from the centre of α and γCDP cavity, which is an indication that the majority of the SH molecules were distributed in the proximity of the cavity in the bulk solutions and the possibility that one SH molecule entered α and γCDP cavity (corresponding to a radial distance below 1 nm) was minimal, compared to the βCDP. These findings are in contrast to those of previous studies (Oishi et al., 2008; Shakalisava and Regan, 2006; Tang et al., 2018), where the complex ratio of 1:1 or 1:2 was reported for γCD, determined by fluorescence intensity and molecular docking. One significant difference between the MD simulation performed in this study and the literature is the chemical structure of the CD cavity, which can explain the contrary result. In fact, MD simulations were performed using a more complex system containing cross-linked CD molecules, where the cross-linker attached to the CD cavity can affect the distribution of SH molecules around the γCDP cavity and cause a major hindrance to the inclusion complex formation as observed for βCDP in a previous study (Lin et al., 2024a).

To better elucidate the contribution of CD types on the interaction with SH molecules and the dynamics of the inclusion complexation, the spatial distribution of SH molecules from the centre of the α, β and γCDP cavities over time was investigated (see Fig. 9).

The comparison of the spatial distribution over time of SH molecules from the CD cavity center in Fig. 9 revealed that CD type affected strongly the residence time of SH molecules in the cavity. Notably, the shortest distance of SHs molecules (specifically estrogens and P) from the cavity was observed for βCDP (distance between 0.6 and 4 nm) in the full simulation time of 90 nanoseconds, while in the case of γ and αCDP, the majority of the SH molecules were distributed at larger distances (6 to 9 nm) and the inclusion complex appeared mostly after about 40 nanoseconds for a short time (see Fig. S13). The radial distribution is consistent with the interaction dynamics shown in Fig. S14, where it was observed that E2 molecules were closer to the βCD cavity and the

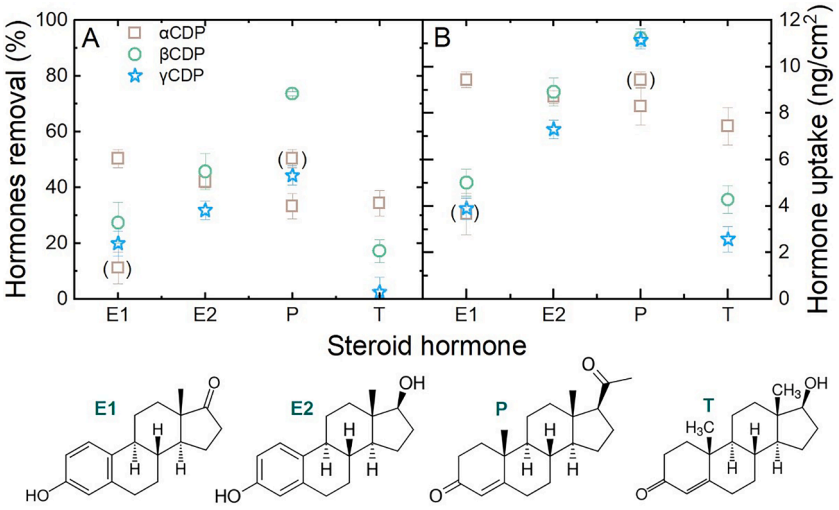

Fig. 7. A) Hormone removal and B) uptake using CNM with different CD types (3.8 mL/min, 22.5 ± 1.7 °C, pH 8.1 ± 0.2, 1 mM $NaHCO_3$, 10 mM NaCl, SHs 100 ng/L). Data for βCD are adapted from (Imbrogno et al. 2024a). Data in brackets are repeated experiments.

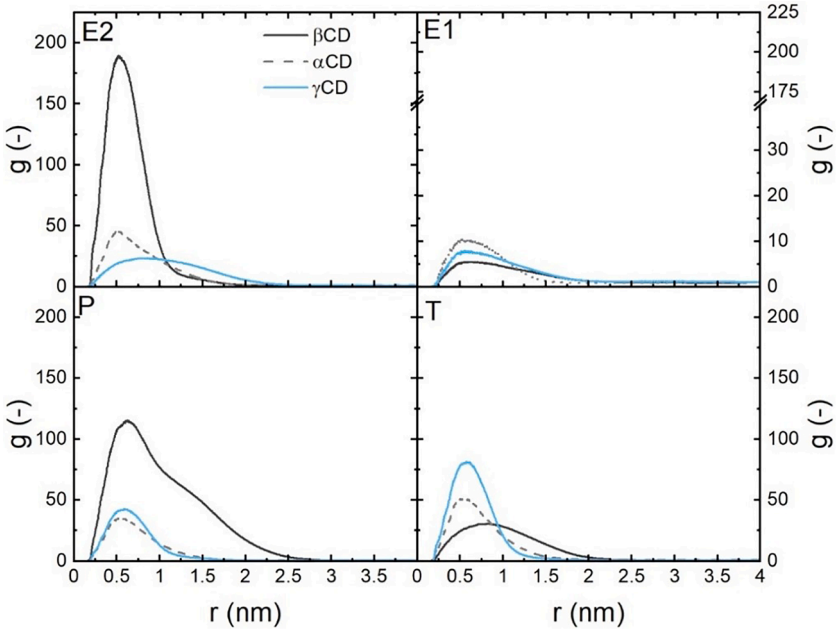

Fig. 8. Cumulative radial distribution function (g) of 10 SH molecules around one cross linked α, β, and γCDP molecule.

formation of hydrogen bonding occurred in proximity of the cavity, while for α and γCD E2 molecules were weakly distributed in proximity of the CD cavity. These findings revealed that inclusion complex formation was stronger and more stable over time for βCDP, while in the case of α and γCDP, most of the SH molecules remained in the bulk solutions and interacted weakly with the inner CD cavity, resulting in less stable inclusion complex formation.

Previous studies reported that de-solvation and interaction energies are the two main energetic steps controlling the complexation of the guest molecule with a macrocyclic host (Abarca et al., 2016; Buchwald, 2002; Gholami et al., 2024). The de-solvation and interaction energies involved in the formation of the inclusion complex of E2 with α, β and γCDP were determined to elucidate the energetic limiting step for the three CD types. Surprisingly, QC calculation revealed that γCDP provided the highest interaction energy of −11.7 kcal/mol, followed by αCDP (−8.9 kcal/mol) and βCDP (−4.9 kcal/mol). A similar interaction energy for inclusion complexation of βCD with E2 (−6.1 kcal/mol) was obtained in another study (Lin et al., 2022) by quantum calculation, which was attributed mainly to hydrophobic and hydrogen bonding interactions. The interaction energy values showed a more stable and stronger complex with γCDP compared to α and βCDP, which is not consistent with the experimental results of E2 removal and the broader spatial distribution observed in MD simulation.

To understand this discrepancy, it is important to highlight that the interaction energy was determined in the gas phase (absence of water molecules), which means that only the CD macrocyclic host and E2 molecules were considered in the calculation, while the spatial distribution as well as the experimental filtration were performed in water. Studies in the literature reported that hydration of CD occurs in water by hydrogen bonding interactions of water molecules with the OH groups in the cavity (Ganjali Koli and Fogolari, 2023; Raffaini and Ganazzoli, 2007; Sandilya et al., 2020; Vicatos et al., 2022). The de-solvation energy to remove solvent molecules from the vicinity of the interaction interface revealed a trend opposite to the interaction energy. Indeed, the

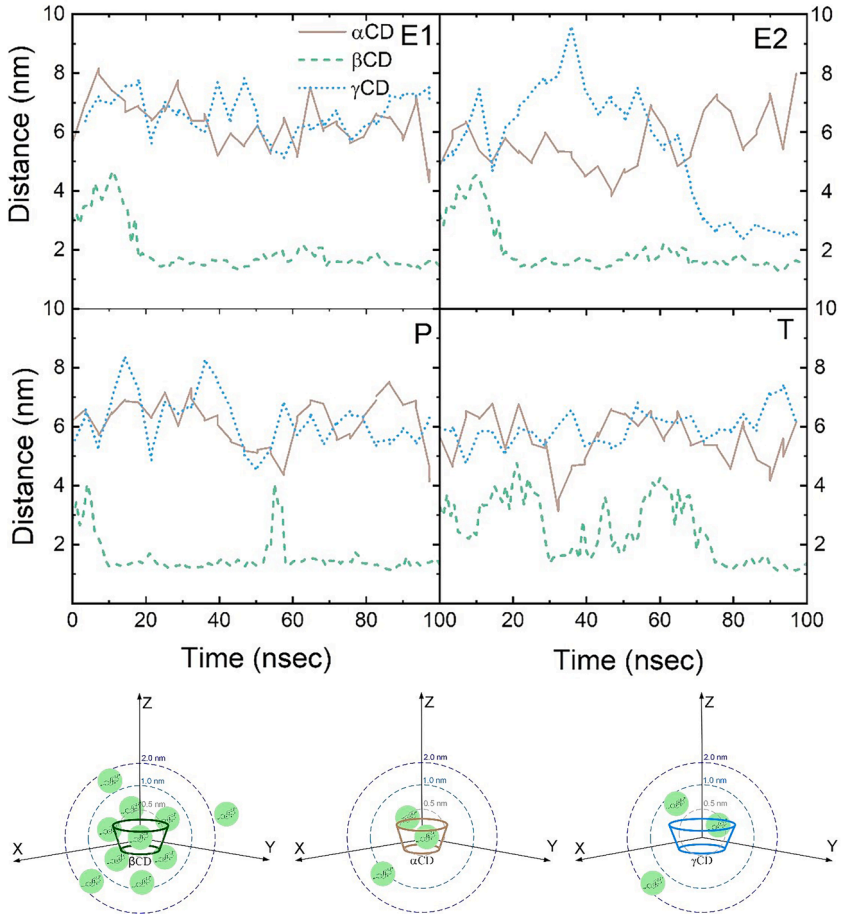

Fig. 9. Top: Cumulative distance of 10 SHs molecules from the center of the CD cavity over time. Bottom:3D schematics of SHs spatial distribution and inclusion complexation for α, β and γCDs. MD data for βCD are adapted from Imbrogno et al. (2024a). MD data of the 10 SHs molecules are in Fig. S13.

highest de-solvation energy was obtained for γCDP (+8.3 kcal/mol), while similar values of +5.6 and 6.0 kcal/mol were obtained for α and βCDP, respectively. This is consistent with a study by Pinjari et al. (2006), who performed an electrostatic potential topography investigation of the CD structure and found a more polar cavity for γCDP. The highest energy of de-solvation (release of water molecules from the cavity) means that this is the energetic limiting step for γCDP, which hinders the subsequent formation of the inclusion complex with E2. This is consistent with the wider spatial distribution of E2 molecules from the centre of the γCDP cavity (Fig. 9) when MD simulation was performed in the presence of water and the lower E2 removal determined experimentally during filtration (Fig. 7). In the case of α and βCDP, similar and lower de-solvation energy is required, while the interaction energy is expected to be the energetic limiting step. In this case, it was expected to have a stronger interaction energy for βCDP, compared to αCDP. However, the QC calculation showed that the interaction energy is more negative for α CDP (−8.9 Kcal/mol) compared to βCDP (−4.9 Kcal/mol), indicating that the inclusion complex is stronger for αCDP. This finding is in contrast to the radial spatial distribution of E2 molecules, which is wider for αCDP (Fig. 9) while a similar experimental E2 removal was observed for α and βCDP (46 and 42 %, respectively). The interaction energy with E2 molecules involves mostly hydrophobic and hydrogen-bonding interactions (Lin et al., 2022). A previous study (Pinjari et al., 2006) reported that hydrogen bonding interaction with αCD occurs mostly with the primary OH groups in the glucose unit (bottom of the ring in Fig. 1), which promotes interaction with the external surface of the CD, while for β and γCDP the hydrogen bonding interactions involves predominantly the secondary OH groups (top of the ring), facilitating the penetration into the cavity. This can justify the wider spatial distribution of E2 molecules in MD simulation, despite the stronger interaction energy obtained for αCDP.

3.6. Contribution of CD type on composite membrane saturation

E2 removal and uptake by the CNM membranes containing α, β and γCDP were investigated at different hormone concentrations to evaluate whether the CD type affects the membrane adsorption capacity. The removal and uptake are reported in Fig. 10A and B.

E2 uptake increased linearly with the increase of feed concentration irrespective of the CD type (Fig. 10B), indicating that membrane saturation was not reached under the tested experimental conditions. This result highlights that CD type is not a controlling parameter of membrane saturation during filtration as indicated by the similar trend observed on E2 removal. This is a plausible result given the similar trend of the breakthrough curve in Fig. S9, where an equilibrium was reached faster at the higher concentrations of 100 and 1000 μg/L, corresponding to the lower E2 removal.

3.7. Steroid hormone removal under limiting factors

The flux (hence, the hydraulic residence time) and the nanofiber matrix thickness (hence, surface area for adsorption) are the two main limiting parameters controlling E2 removal and uptake (Imbrogno et al., 2024a). These two limiting factors were investigated for α, β and γCDP to determine whether the variation of E2 removal and uptake is dependent on the CD type. The results are reported in Fig. 11 A, B for different fluxes and C-D for different nanofiber matrix thicknesses (that is, the number of electrospinning cycles).

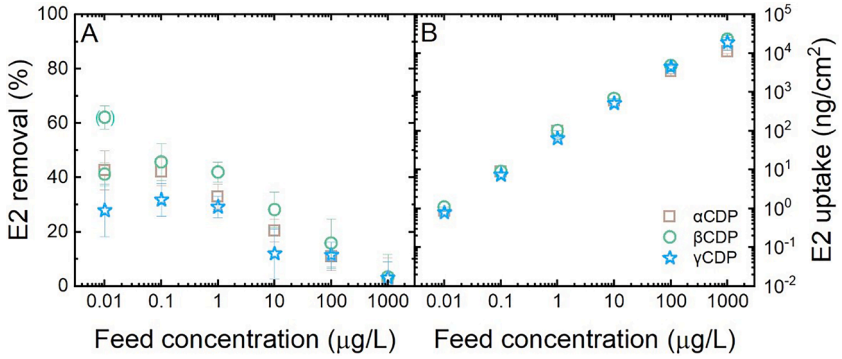

Fig. 10. E2 removal and uptake as a function of feed concentration using the CNM with different types of CD (3.8 mL/min, 22.5 ± 1.7 °C, pH 8.1 ± 0.2, 1 mM $NaHCO_3$, 10 mM NaCl, pH 8.1 ± 2, E2 100 ng/L). Data for βCD are adapted from Imbrogno et al. (2024a).

Increasing the flux from 158 to 1260 L/m^2.h (a factor of 8) caused a decrease of E2 removal by 1.6 and 2 times, for β and αCDP, respectively, and 2 times for γCDP, which is consistent with the reduction of E2 uptake by almost 2 times. This result highlights that the HRT is a limiting factor for the E2 uptake irrespective of the CD type. A similar trend with varying HRT was observed in previous studies where adsorbing materials, such as polymer spherical activated carbon, carbon nanotubes and βCD covalently attached on MF membranes, were applied in filtration for the removal of SHs, pesticides and bisphenol A (Nguyen et al., 2021; Tagliavini and Schäfer, 2018; Trinh and Schäfer, 2024; Wang et al., 2020). In another study (Fan et al., 2019) it was reported an increase of adsorption rate with increase of feed flow rate (hence flux) and a decrease of adsorption capacity because of the shorter interaction time between bisphenol A and the CD adsorbent molecules immobilized in a chitosan/poly-vinyl alcohol nanofiber matrix, which is consistent with the results reported in Fig. 11C.

When the nanofiber matrix thickness increased from 180 to 420 μm, E2 removal increased by almost 3 times for β and γCDP and by almost 2 times for αCDP. The increase was more significant at a thickness below 300 μm, while remaining constant with further increase of the nanofiber matrix thickness above 300 μm. This is consistent with the E2 uptake, which remained unchanged in the range of 8.2 to 9.5 ng/cm^2 at nanofiber matrix thickness from 210 to 420 μm. Similar results were obtained in previous studies, where the increase of polymer spherical activated carbon layer (hence the external surface area) in composed UF membrane resulted in insignificant enhancement of SHs and pesticides (glyphosate) removal (Tagliavini et al., 2020; Trinh and Schäfer, 2024). Another study (Tagliavini et al., 2023) explained that the axial dispersion rate is the parameter controlled by the adsorbent layer thickness, resulting in enhanced dispersive transport at higher thickness and reduced adsorption rate. This finding supports the experimental trend observed for E2 removal and uptake as a function of nanofiber matrix thickness. The dominance of the axial dispersion rate at higher nanofiber matrix thickness is evident in the change of the breakthrough curve shape (see Fig. S10), which became flatter at thickness above 210 μm. Previous studies (Weber and Liu, 1980; Worch, 2004) on the mass transport in bed column, reported that a flatter breakthrough curve occurs when the intraparticle mass transport (in this case the mass

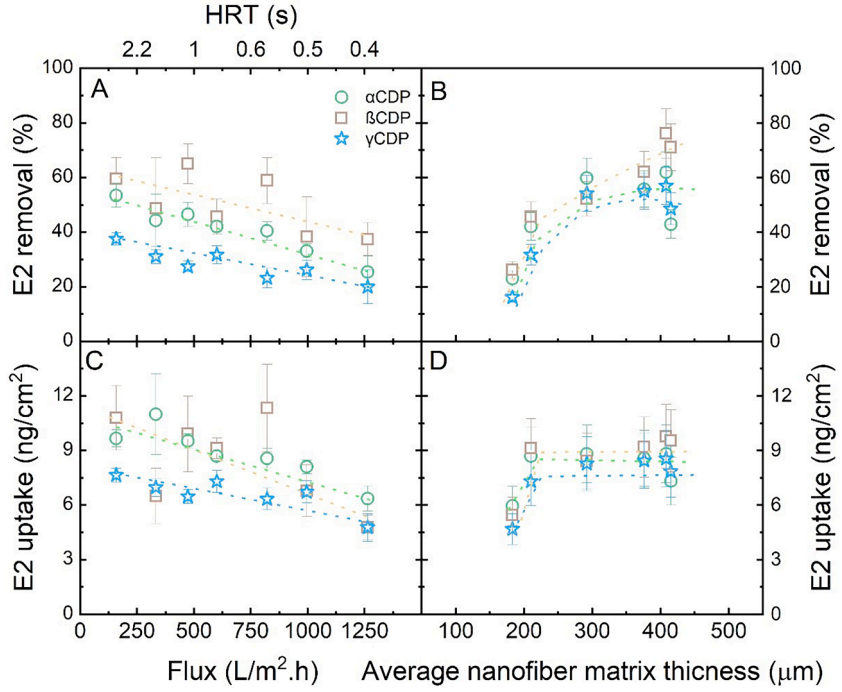

Fig. 11. E2 removal and uptake as a function of (A, B) flow rate and (C, D) matrix thickness with different CNMs (22.5 ± 1.7 °C, pH 8.1 ± 0.2, 1 mM $NaHCO_3$, 10 mM NaCl and 100 ng/L of E2, 15 g/cm^2 CDP). HRT is reported as the average value from experiments with CNMs and α, β, γCDP. The average nanofiber matrix thickness is calculated by averaging the nanofiber matrix thickness of α, β, γCDP. Data for βCD are adapted from Imbrogno et al. (2024a).

transport in the void space between nanofibers) is reduced, which is consistent with the findings observed in this study at higher nanofiber matrix thickness. These results revealed that the highest possible removal of 71 % and uptake of 9.5 ng/cm^2 can be achieved with βCDP at a flux of 600 L/m^{2}h (HRT of 0.8 s), while a lower removal of about 49 % can be achieved with α and γCD, at similar limiting parameters of nanofiber matrix thickness and flux.

4. Conclusions

The contribution of CD type on SHs removal, uptake and inclusion complexation affinity was investigated by entrapping different CDs, namely α, β and γCD into a CNM membrane.

Interestingly, the CD type played a major role controlling SH interactions and the complexation dynamics. In the case of αCDP, a similar removal of P, T and estrogens E1 and E2 (33, 34, 42 and 50 %, respectively) was observed, while for β and γCDP, the removal and uptake were dependent on SH type. Indeed, the highest removal of 74 % and uptake of 11.1 ng/cm^2 was obtained for P with βCD, followed by E2 (46 %) and E1 (27 %), while the lowest removal and uptake of 3 % and 13 % was observed for T when γ and βCDP were used, respectively. MD simulation on the radial spatial distribution over time of SH molecules from the CD cavity, revealed that in the case of γ and αCD SH molecules were distributed mainly at larger distances (6 to 9 nm) from the CD cavity and the inclusion complexation appeared for a short time independently of SH type. In contrast, βCDP showed a stronger and more stable inclusion complexation over time, especially for P and estrogens (E1 and E2). This was attributed to higher de-solvation energy for γCDP (+8.3 kcal/mol) compared to α and βCDP (5.6 and 6 kcal/mol), which provided more hindrance to the release of the water molecules interface of CD molecule and hormone and subsequent formation of the inclusion complex with SHs. In the case of α and βCDP, despite the stronger interaction energy of αCDP (−8.9 kcal/mol) a similar E2 removal was observed under experimental filtration and a wider spatial distribution was obtained from MD simulation. This discrepancy was attributed to a different hydrogen bonding interactions which occurred mostly at the external surface for αCDP with the secondary OH groups.

In conclusion, the CD type is an important parameter to control SH uptake from water with CNM membrane containing CD molecules. Among the three CDs, βCD provides the strongest affinity to form selective and more stable inclusion complexation with steroid hormones, especially with estrogens and progesterone.

CRediT authorship contribution statement

Alessandra Imbrogno: Writing – original draft, Visualization, Validation, Methodology, Investigation, Formal analysis, Data curation, Conceptualization. **Han Ya Lin:** Writing – review & editing, Visualization, Validation, Methodology, Investigation, Formal analysis, Data curation. **Akhil Gopalakrishnan:** Writing – review & editing, Visualization, Validation, Formal analysis. **Babak Minofar:** Writing – review & editing, Software, Methodology, Data curation. **Andrea I. Schäfer:** Writing – review & editing, Supervision, Resources, Funding acquisition, Conceptualization.

Declaration of competing interest

The authors declare that they have no known competing financial interests or personal relationships that could have appeared to influence the work reported in this paper.

Data availability

Data will be made available on request.

Acknowledgements

The Helmholtz Association is thanked for the project funding in form of the Recruitment Initiative for IAMT. Millipore (Bedford, USA) provided the UF membrane and BMBF CANDECT funded for the development of electrospinning methodology. The BMBF project RealMethod provided salary to Han-Ya Lin as well as project funding, while the project ‘e-Infrastruktura CZ’ (e-INFRA LM2018140), the program ‘Projects of Large Research Development, and Innovations Infrastructures’ and the grant 21-15936S from the Grant Agency of the Czech Republic are thanked for computational resources. Rebat Karki is thanked for performing the filtration and static adsorption experiments with α and βCD. Dr. Justine Nyarige and Dr. Dimitry Busko (Institute of Microstructure Technology, IMT) carried out SEM imaging and provided liquid nitrogen, respectively. Dr. David Řeha (VŠB-Technical University of Ostrava, Czech Republic) supported with calculations of interaction energy and related discussions.

Supplementary materials

Supplementary material associated with this article can be found, in the online version, at doi:10.1016/j.watres.2024.122543.

References

Abarca, R.L., Rodríguez, F.J., Guarda, A., Galotto, M.J., Bruna, J.E., 2016. Characterization of beta-cyclodextrin inclusion complexes containing an essential oil component. Food Chem. 196, 968–975.
Adeel, M., Song, X., Wang, Y., Francis, D., Yang, Y., 2017. Environmental impact of estrogens on human, animal and plant life: a critical review. Environ. Int. 99, 107–119.
Alsbaiee, A., Smith, B.J., Xiao, L., Ling, Y., Helbling, D.E., Dichtel, W.R., 2016. Rapid removal of organic micropollutants from water by a porous β-cyclodextrin polymer. Nature 529 (7585), 190–194.
Askari, A., Nabavi, S.R., Omrani, A., 2023. Parametric optimization of poly (ether sulfone) electrospun membrane for effective oil/water separation. Polym. Eng. Sci. 63 (12), 4285–4298.
Baker, R.W., 2004. Membrane Technology and Applications. John Wiley & Sons.
Bhandari, R.K., Deem, S.L., Holliday, D.K., Jandegian, C.M., Kassotis, C.D., Nagel, S.C., Tillitt, D.E., Vom Saal, F.S., Rosenfeld, C.S., 2015. Effects of the environmental estrogenic contaminants bisphenol A and 17α-ethinyl estradiol on sexual development and adult behaviors in aquatic wildlife species. Gen. Comp. Endocrinol. 214, 195–219.
Bhatt, P., Bhandari, G., Bilal, M., 2022. Occurrence, toxicity impacts and mitigation of emerging micropollutants in the aquatic environments: recent tendencies and perspectives. J. Environ. Chem. Eng. 10 (3), 107598.
Bilal, M., Barceló, D., Iqbal, H.M., 2021. Occurrence, environmental fate, ecological issues, and redefining of endocrine disruptive estrogens in water resources. Sci. Total Environ. 800, 149635.
Boys, S.F., Bernardi, F., 1970. The calculation of small molecular interactions by the differences of separate total energies. Some procedures with reduced errors. Mol. Phys. 19 (4), 553–566.
Bridle, H.L., Heringa, M.B., Schäfer, A.I., 2016. Solid-phase microextraction to determine micropollutant-macromolecule partition coefficients. Nat. Protoc. 11 (8), 1328–1344.
Buchwald, P., 2002. Complexation thermodynamics of cyclodextrins in the framework of a molecular size-based model for nonassociative organic liquids that includes a modified hydration-shell hydrogen-bond model for water. J. Phys. Chem. B 106 (27), 6864–6870.
Celebioglu, A., Topuz, F., Uyar, T., 2019. Water-insoluble hydrophilic electrospun fibrous mat of cyclodextrin–epichlorohydrin polymer as highly effective sorbent. ACS Appl. Polym. Mater. 1 (1), 54–62.
Cheng, D., Ngo, H.H., Guo, W., Chang, S.W., Nguyen, D.D., Liu, Y., Wei, Q., Wei, D., 2020. A critical review on antibiotics and hormones in swine wastewater: water pollution problems and control approaches. J. Hazard. Mater. 387, 121682.
Dalanta, F., Handoko, D.T., Hadiyanto, H., Kusworo, T.D., 2023. Recent implementations of process intensification strategy in membrane-based technology: a review. Chem. Eng. Res. Des.
de Oliveira, D.M., Ben-Amotz, D., 2019. Cavity hydration and competitive binding in methylated β-cyclodextrin. J. Phys. Chem. Lett. 10 (11), 2802–2805.
Del Valle, E.M., 2004. Cyclodextrins and their uses: a review. Process Biochem. 39 (9), 1033–1046.
Diamanti-Kandarakis, E., Bourguignon, J.P., Giudice, L.C., Hauser, R., Prins, G.S., Soto, A.M., Zoeller, R.T., Gore, A.C., 2009. Endocrine-disrupting chemicals: an Endocrine Society scientific statement. Endocr. Rev. 30 (4), 293–342.
Ding, J., Steiner, T., Saenger, W., 1991. Structure of the γ-cyclodextrin–1-propanol–17H2O inclusion complex. Acta Crystallogr. B Struct. Sci. 47 (5), 731–738.

Dong, Z., Tagliavini, M., Darmadi, J., Trouillet, V., Schäfer, A.I., Levkin, P.A., 2020. Regeneration of β-Cyclodextrin based membrane by photodynamic disulfide exchange—steroid hormone removal from water. Adv. Mat. Interf. 7 (22), 1902100.
European Parliament (2022) Commission implementing decision (EU) 2022/679 of 19 January 2022 establishing a watch list of substances and compounds of concern for water intended for human consumption as provided for in directive (EU) 2020/2184 of the European parliament and of the council (notified under document C(2022) 142).
Fan, J.P., Luo, J.J., Zhang, X.H., Zhen, B., Dong, C.Y., Li, Y.C., Shen, J., Cheng, Y.T., Chen, H.P., 2019. A novel electrospun β-CD/CS/PVA nanofiber membrane for simultaneous and rapid removal of organic micropollutants and heavy metal ions from water. Chem. Eng. J. 378, 122232.
Frisch, M., 2009. Gaussian 09, Revision d. 01. Gaussian. Inc. Wallingford CT 201.
Ganjali Koli, M., Fogolari, F., 2023. Exploring the role of cyclodextrins as a cholesterol scavenger: a molecular dynamics investigation of conformational changes and thermodynamics. Sci. Rep. 13 (1), 21765.
Gholami, R., Azizi, K., Ganjali Koli, M., 2024. Unveiling the dynamic and thermodynamic interactions of hydrocortisone with β-cyclodextrin and its methylated derivatives through insights from molecular dynamics simulations. Sci. Rep. 14 (1), 12495.
Ghosh, S., Badruddoza, A.Z.M., Hidajat, K., Uddin, M.S., 2013. Adsorptive removal of emerging contaminants from water using superparamagnetic Fe3O4 nanoparticles bearing aminated β-cyclodextrin. J. Environ. Chem. Eng. 1 (3), 122–130.
Gidwani, B., Vyas, A., 2014. Synthesis, characterization and application of Epichlorohydrin-β-cyclodextrin polymer. Colloids Surf. B Biointerfaces 114, 130–137.
Guo, Y.Z., Gao, F., Wang, Z., Liu, Y.A., Hu, W.B., Yang, H., Wen, K., 2021. Highly branched pillar [5]arene-derived porous aromatic frameworks (PAFs) for removal of organic pollutants from water. ACS Appl. Mater. Interfaces 13 (14), 16507–16515.
Hemine, K., Skwierawska, A., Kernstein, A., Kozłowska-Tylingo, K., 2020. Cyclodextrin polymers as efficient adsorbents for removing toxic non-biodegradable pimavanserin from pharmaceutical wastewaters. Chemosphere 250, 126250.
Hess, B., Kutzner, C., Van Der Spoel, D., Lindahl, E., 2008. GROMACS 4: algorithms for highly efficient, load-balanced, and scalable molecular simulation. J. Chem. Theory Comput. 4 (3), 435–447.
Heydari, A., Mehrabi, F., Shamspur, T., Sheibani, H., Mostafavi, A., 2018. Encapsulation and controlled release of Vitamin B2 using peracetyl-β-cyclodextrin polymer-based electrospun nanofiber Scaffold. Pharm. Chem. J. 52 (1), 19–25.
Homaeigohar, S.S., Buhr, K., Ebert, K., 2010. Polyethersulfone electrospun nanofibrous composite membrane for liquid filtration. J. Membr. Sci. 365 (1–2), 68–77.
Imbrogno, A., Lin, H.Y., Minofar, B., Schäfer, A.I., 2024a. Nanofiber composite ultrafiltration membrane functionalized with cross-linked β-cyclodextrin for steroid hormone micropollutant removal. J. Membr. Sci. 691, 122212.
Imbrogno, A., Nguyen, M.N., Schäfer, A.I., 2024b. Tutorial review of error evaluation in experimental water research at the example of membrane filtration. Chemosphere, 141833.
Imbrogno, A., Schäfer, A.I., 2021. Micropollutants breakthrough curve phenomena in nanofiltration: impact of operational parameters. Sep. Purif. Technol. 267, 118406.
Jiang, L., Liu, Y., Liu, S., Hu, X., Zeng, G., Hu, X., Liu, S., Liu, S., Huang, B., Li, M., 2017. Fabrication of β-cyclodextrin/poly (l-glutamic acid) supported magnetic graphene oxide and its adsorption behavior for 17β-estradiol. Chem. Eng. J. 308, 597–605.
Kamaraj, M., Babu, P.S., Shyamalagowri, S., Pavithra, M., Aravind, J., Kim, W., Govarthanan, M., 2024. β-cyclodextrin polymer composites for the removal of pharmaceutical substances, endocrine disruptor chemicals, and dyes from aqueous solution–a review of recent trends. J. Environ. Manag. 351, 119830.
Kamilya, T., Yadav, M.K., Ayoob, S., Tripathy, S., Bhatnagar, A., Gupta, A.K., 2023. Emerging impacts of steroids and antibiotics on the environment and their remediation using constructed wetlands: a critical review. Chem. Eng. J. 451, 138759.
Kayaci, F., Aytac, Z., Uyar, T., 2013. Surface modification of electrospun polyester nanofibers with cyclodextrin polymer for the removal of phenanthrene from aqueous solution. J. Hazard. Mater. 261, 286–294.
Lee, J.H., Kwak, S.-Y., 2019. Rapid adsorption of bisphenol A from wastewater by β-cyclodextrin-functionalized mesoporous magnetic clusters. App. Surf. Sci. 467, 178–184.
Lewis, K.M., Archer, R.D., 1979. pKa values of estrone, 17 beta-estradiol and 2-methoxyestrone. Steroids 34 (5), 485–499.
Lin, H.Y., Imbrogno, A., Gopalakrishnan, A., Minofar, B., Schäfer, A.I., 2024a. Role of cyclodextrin cross-linker type on steroid hormone micropollutant removal from water using composite nanofiber membrane. ACS Appl. Polym. Mater.
Lin, Q., Ding, X.L., Hou, Y.S., Ali, W., Li, Z.C., Han, X., Meng, Z., Sun, Y., Liu, Y., 2024b. Adsorption and separation technologies based on supramolecular macrocycles for water treatment. Eco-Environ. Health.
Lin, Z.Y., Wang, X.X., Kou, S.B., Shi, J.H., 2022. Exploring the inclusion interaction of estradiol with β-CD and HP-β-CD with the help of molecular dynamics simulation as well as multi-spectroscopic approaches. Spectrochim. Acta A Mol. Biomol. Spectrosc. 269, 120764.
Lin, Q., Wu, Y., Jiang, X., Lin, F., Liu, X., Lu, B., 2019. Removal of bisphenol A from aqueous solution via host-guest interactions based on beta-cyclodextrin grafted cellulose bead. Int. J. Bio. Macromol. 140, 1–9.
Lu, Q., Li, N., Li, J., 2020. Supramolecular adsorption of cyclodextrin/polyvinyl alcohol film for purification of organic wastewater. J. Polym. Eng. 40 (2), 158–172.
Ma, J., Zhang, Y., Zhao, B., Jia, Q., 2020. Supramolecular adsorbents in extraction and separation techniques–a review. Anal. Chim. Acta 1122, 97–113.
Marenich, A.V., Cramer, C.J., Truhlar, D.G., 2009. Universal solvation model based on solute electron density and on a continuum model of the solvent defined by the bulk dielectric constant and atomic surface tensions. J. Phys. Chem. B 113 (18), 6378–6396.
Martínez, J.M., Martínez, L., 2003. Packing optimization for automated generation of complex system's initial configurations for molecular dynamics and docking. J. Comput. Chem. 24 (7), 819–825.
Martínez, L., Andrade, R., Birgin, E.G., Martínez, J.M., 2009. PACKMOL: a package for building initial configurations for molecular dynamics simulations. J. Comput. Chem. 30 (13), 2157–2164.
Morin-Crini, N., Winterton, P., Fourmentin, S., Wilson, L.D., Fenyvesi, E., Crini, G., 2018. Water-insoluble β-cyclodextrin–epichlorohydrin polymers for removal of pollutants from aqueous solutions by sorption processes using batch studies: a review of inclusion mechanisms. Prog. Polym. Sci. 78, 1–23.
Moulahcene, L., Skiba, M., Senhadji, O., Milon, N., Benamor, M., Lahiani-Skiba, M., 2015. Inclusion and removal of pharmaceutical residues from aqueous solution using water-insoluble cyclodextrin polymers. Chem. Eng. Res. Des. 97, 145–158.
Mulder, J., 2012. Basic Principles of Membrane Technology. Springer Science & Business Media.
Nguyen, M.N., Trinh, P.B., Burkhardt, C.J., Schäfer, A.I., 2021. Incorporation of single-walled carbon nanotubes in ultrafiltration support structure for the removal of steroid hormone micropollutants. Sep. Purif. Technol. 264, 118405.
Nielsen, R., Kingshott, P., Uyar, T., Hacaloglu, J., Larsen, K.L., 2011. Characterization of β-cyclodextrin modified SiO2. Surf. Interface Anal. 43 (5), 884–892.
Nure, J.F., Nkambule, T.T., 2023. The recent advances in adsorption and membrane separation and their hybrid technologies for micropollutants removal from wastewater. J. Ind. Eng. Chem. 126, 92–114.
Oishi, K., Moriuchi, A., 2010. Removal of dissolved estrogen in sewage effluents by β-cyclodextrin polymer. Sci. Total Environ. 409 (1), 112–115.
Oishi, K., Toyao, K., Kawano, Y., 2008. Suppression of estrogenic activity of 17β-estradiol by β-cyclodextrin. Chemosphere 73 (11), 1788–1792.
Ozelcaglayan, E.D., Parker, W., 2023. β-Cyclodextrin functionalized adsorbents for removal of organic micropollutants from water. Chemosphere 320, 137964.
Pinjari, R.V., Joshi, K.A., Gejji, S.P., 2006. Molecular electrostatic potentials and hydrogen bonding in α-, β-, and γ-cyclodextrins. J. Phys. Chem. A 110 (48), 13073–13080.
Raffaini, G., Ganazzoli, F., 2007. Hydration and flexibility of α-, β-, γ-and δ-cyclodextrin: a molecular dynamics study. Chem. Phys. 333 (2–3), 128–134.
Rana, V.K., Kissner, R., Gaspard, S., Levalois-Grützmacher, J., 2016. Cyclodextrin as a complexation agent in the removal of chlordecone from water. Chem. Eng. J. 293, 82–89.
Rekharsky, M.V., Inoue, Y., 1998. Complexation thermodynamics of cyclodextrins. Chem. Rev. 98 (5), 1875–1918.
Renard, E., Deratani, A., Volet, G., Sebille, B., 1997. Preparation and characterization of water soluble high molecular weight β-cyclodextrin-epichlorohydrin polymers. Eur. Polym. J. 33 (1), 49–57.
Romita, R., Rizzi, V., Semeraro, P., Gubitosa, J., Gabaldón, J.A., Gorbe, M.I.F., López, V. M.G., Cosma, P., Fini, P., 2019. Operational parameters affecting the atrazine removal from water by using cyclodextrin based polymers as efficient adsorbents for cleaner technologies. Environ. Technol. Innov. 16, 100454.
Sadlej-Sosnowska, N., 1997. Influence of the structure of steroid hormones on their association with cyclodextrins: a high-performance liquid chromatography study. J. Incl. Phenom. Mol. Recognit. Chem. 27, 31–40.
Sandilya, A.A., Natarajan, U., Priya, M.H., 2020. Molecular view into the cyclodextrin cavity: structure and hydration. ACS Omega 5 (40), 25655–25667.
Saravanan, A., Deivayanai, V., Kumar, P.S., Rangasamy, G., Hemavathy, R., Harshana, T., Gayathri, N., Alagumalai, K., 2022. A detailed review on advanced oxidation process in treatment of wastewater: mechanism, challenges and future outlook. Chemosphere 308, 136524.
Schäfer, A.I., Akanyeti, I., Semião, A.J., 2011. Micropollutant sorption to membrane polymers: a review of mechanisms for estrogens. Adv. Colloid Interface Sci. 164 (1), 100–117.
Shakalisava, Y., Regan, F., 2006. Determination of association constants of inclusion complexes of steroid hormones and cyclodextrins from their electrophoretic mobility. Electrophoresis 27 (15), 3048–3056.
Sikder, M.T., Rahman, M.M., Jakariya, M., Hosokawa, T., Kurasaki, M., Saito, T., 2019. Remediation of water pollution with native cyclodextrins and modified cyclodextrins: a comparative overview and perspectives. Chem. Eng. J. 355, 920–941.
Spencer, J., He, Q., Ke, X., Wu, Z., Fetter, E., 1998. Complexation of inorganic anions and small organic molecules with alpha-cyclodextrin in water. J. Solut. Chem. 27, 1009–1019.
Szejtli, J., 1998. Introduction and general overview of cyclodextrin chemistry. Chem. Rev. 98 (5), 1743–1754.
Tagliavini, M., Nguyen, M.N., Schäfer, A.I., 2023. Predicting steroid hormone removal in a thin activated carbon layer coupled with ultrafiltration. Chem. Eng. J. 462, 142125.
Tagliavini, M., Schäfer, A.I., 2018. Removal of steroid micropollutants by polymer-based spherical activated carbon (PBSAC) assisted membrane filtration. J. Hazard. Mater. 353, 514–521.
Tagliavini, M., Weidler, P.G., Njel, C., Pohl, J., Richter, D., Böhringer, B., Schäfer, A.I., 2020. Polymer-based spherical activated carbon–ultrafiltration (UF-PBSAC) for the adsorption of steroid hormones from water: material characteristics and process configuration. Water Res. 185, 116249.
Tang, P., Sun, Q., Suo, Z., Zhao, L., Yang, H., Xiong, X., Pu, H., Gan, N., Li, H., 2018. Rapid and efficient removal of estrogenic pollutants from water by using beta-and gamma-cyclodextrin polymers. Chem. Eng. J. 344, 514–523.

Tian, B., Hua, S., Tian, Y., Liu, J., 2021. Cyclodextrin-based adsorbents for the removal of pollutants from wastewater: a review. Environ. Sci. Pollut. Res. 28 (2), 1317–1340.
Trasande, L., Zoeller, R.T., Hass, U., Kortenkamp, A., Grandjean, P., Myers, J.P., DiGangi, J., Bellanger, M., Hauser, R., Legler, J., 2015. Estimating burden and disease costs of exposure to endocrine-disrupting chemicals in the European Union. J. Clin. Endocrinol. Metab. 100 (4), 1245–1255.
Trinh, P.B., Schäfer, A.I., 2024. Removal of glyphosate (GLY) and aminomethylphosphonic acid (AMPA) by ultrafiltration with permeate-side polymer-based spherical activated carbon (UF–PBSAC). Water Res. 250, 121021.
Uebele, S., Goetz, T., Ulbricht, M., Schiestel, T., 2022. Mixed-matrix membrane adsorbers for the simultaneous removal of different pharmaceutical micropollutants from water. ACS Appl. Polym. Mater. 4 (3), 1705–1716.
Van Der Spoel, D., Lindahl, E., Hess, B., Groenhof, G., Mark, A.E., Berendsen, H.J., 2005. GROMACS: fast, flexible, and free. J. Comput. Chem. 26 (16), 1701–1718.
Vicatos, A.I., Hoossen, Z., Caira, M.R., 2022. Inclusion complexes of the steroid hormones 17β-estradiol and progesterone with β-and γ-cyclodextrin hosts: syntheses, X-ray structures, thermal analyses and API solubility enhancements. Beilstein J. Org. Chem. 18 (1), 1749–1762.
Wang, Z., Cui, F., Pan, Y., Hou, L., Zhang, B., Li, Y., Zhu, L., 2019. Hierarchically micro-mesoporous β-cyclodextrin polymers used for ultrafast removal of micropollutants from water. Carbohydr. Pol. 213, 352–360.
Wang, Z., Guo, S., Zhang, B., Fang, J., Zhu, L., 2020. Interfacially crosslinked β-cyclodextrin polymer composite porous membranes for fast removal of organic micropollutants from water by flow-through adsorption. J. Hazard. Mater. 384, 121187.
Waring, A.J., 1983. pKa Prediction for Organic Acids and Bases. Chapman and Hall, London. D.D. Perrin, B. Dempsey, and E.P. Serjeant1981. 118 pp. + 31 pp. tables, price £10.95. Analytica Chimica Acta 152, 308.
Weber Jr, W., Liu, K., 1980. Determination of mass transport parameters for fixed-bed adsorbers. Chem. Eng. Commun. 6 (1–3), 49–60.
Worch, E., 2004. Modelling the solute transport under nonequilibrium conditions on the basis of mass transfer equations. J. Contam. Hydrol. 68 (1–2), 97–120.
Wu, C.C., Shields, J.N., Akemann, C., Meyer, D.N., Connell, M., Baker, B.B., Pitts, D.K., Baker, T.R., 2021. The phenotypic and transcriptomic effects of developmental exposure to nanomolar levels of estrone and bisphenol A in zebrafish. Sci. Total Environ. 757, 143736.
Xu, R., Zhang, Z., Deng, C., Nie, C., Wang, L., Shi, W., Lyu, T., Yang, Q., 2023. Micropollutant rejection by nanofiltration membranes: a mini review dedicated to the critical factors and modelling prediction. Environ. Res., 117935
Zeeman, M., 1996. Our stolen future: are we threatening our fertility, intelligence, and survival? A scientific detective story. Bioscience 46 (7), 542–546.
Zhang, J., Nguyen, M.N., Li, Y., Yang, C., Schäfer, A.I., 2020. Steroid hormone micropollutant removal from water with activated carbon fiber-ultrafiltration composite membranes. J. Hazard. Mater. 391, 122020.
Zhao, Y., Truhlar, D.G., 2008. The M06 suite of density functionals for main group thermochemistry, thermochemical kinetics, noncovalent interactions, excited states, and transition elements: two new functionals and systematic testing of four M06-class functionals and 12 other functionals. Theor. Chem. Acc. 120, 215–241.
Zhou, S., Jin, L., Gu, P., Tian, L., Li, N., Chen, D., Marcomini, A., Xu, Q., Lu, J., 2022. Novel calixarene-based porous organic polymers with superfast removal rate and ultrahigh adsorption capacity for selective separation of cationic dyes. Chem. Eng. J. 433, 134442.